

Superconducting properties of ultrathin $\text{Bi}_2\text{Sr}_2\text{CaCu}_2\text{O}_{8+x}$ single crystals

L. X. You,* A. Yurgens, and D. Winkler

*Quantum Device Physics Laboratory,
Department of Microtechnology and Nanoscience,
Chalmers University of Technology, SE-412 96 Göteborg, Sweden*

C. T. Lin and B. Liang

*Max-Planck-Institut für Festkörperforschung,
Heisenbergstrasse 1, D-70569 Stuttgart, Germany*

(Dated: September 1, 2018)

Abstract

We use Ar-ion milling to thin $\text{Bi}_2\text{Sr}_2\text{CaCu}_2\text{O}_{8+x}$ (Bi2212) single crystals down to a few nanometers or one-to-two $(\text{CuO}_2)_2$ layers. With decreasing the thickness, superconducting transition temperature gradually decreases to zero and the in-plane resistivity increases to large values indicating the existence of a superconductor-insulator transition in ultrathin Bi2212 single crystals.

PACS numbers: 74.25.Fy, 74.62.Yb, 74.72.Hs, 74.78.Bz,

*Electronic address: lixing@mc2.chalmers.se

I. INTRODUCTION

Many high-temperature superconductors (HTS) are widely considered as two-dimensional (2D). The cuprate HTS consists of conducting layers of CuO_2 planes separated by poorly conducting or even insulating charge reservoirs. Among the most anisotropic HTS is $\text{Bi}_2\text{Sr}_2\text{CaCu}_2\text{O}_{8+x}$ (Bi2212) compound, where the separating charge reservoir consists of BiO_2 and CaO planes. These build up a relatively large distance (12\AA) between $(\text{CuO}_2)_2$ planes which in turn results in a weak c -axis coupling and strong anisotropy in both the normal and superconducting state. This high anisotropy and the quasi-two-dimensional (2D) character of conductivity and superconductivity of CuO_2 planes result in a number of unusual physical properties and effects, with intrinsic Josephson tunneling standing out as one of the most intriguing one [1].

The Kosterlitz-Thouless (KT) transition which appears substantially below the bulk transition temperature T_{c0} and is associated with the thermal dissociation of vortex-antivortex pairs above a certain temperature T_{KT} is characteristic for a disorder-free 2D superconductor. As the disorder is introduced, T_{KT} can be further suppressed [2], even down to zero at a certain critical disorder strength or below a specific thin-film thickness [3]. Several publications have shown that thin films of different superconducting materials become insulating when their normal-state resistance is larger than the universal quantum resistance $R_q = h/(2e)^2 \approx 6.5 \text{ k}\Omega$ [4, 5, 6], i.e. a superconductor-insulator transition occurs.

The question naturally arises, whether the superconductivity of an isolated $(\text{CuO}_2)_2$ plane is sufficiently robust and is characterized by a non-zero T_{KT} . To provide experimental evidence for this issue is obviously a very difficult and challenging task. The epitaxial cuprate film layers interleaved between buffering thin-film layers has been one way of investigating the superconducting properties of isolated $(\text{CuO}_2)_2$ planes [7, 8, 9, 10]. However, the initial growth of a film involves complicated nucleation processes affected by the lattice mismatch between the film and substrate [11]. For a better lattice matching one can grow buffer layers of non-superconducting Bi2201 between Bi2212 and the substrate [7]. This buffer contains CuO_2 planes and electrically is quite well conducting, which may affect the superconductivity in the ultrathin Bi2212 films on top.

HTS bulk single crystals with perfect crystal structure are routinely grown by many groups [12, 13, 14, 15]. Bi2212 single crystals are widely used in many studies due to their

high anisotropy and the presence of the intrinsic Josephson effect [1]. The thickness of the single crystals is always very large compared with thin films and is difficult to measure or control precisely. However, the indisputable merit of single crystals is that the crystal orientation is perfect in all three dimensions and there are no complications with regard to the nucleation processes or any lattice mismatch characteristic between the thin films and the substrate.

In this work, by using conventional photolithography and Ar-ion milling we could controllably thin down single crystals to any thickness. We see that the superconducting critical temperature T_c does not depend on thickness down to a few nanometers. The superconductivity gradually vanishes on further decrease of the thickness.

II. SAMPLE PREPARATION

Bi2212 single crystals with a typical critical temperature $T_c \sim 85$ K were grown using the traveling solvent floating zone (TSFZ) method [14]. The main fabrication process is similar to the process for fabrication of IJJs' [16, 17, 18].

First, we glue a single crystal of Bi2212 onto a sapphire substrate using polyimide. Then we cleave the crystal using common Scotch tape. Immediately after the cleavage, the single crystal is covered by a 20 nm thin film of CaF_2 followed by 20 nm of gold. Both films are made by physical-vapor deposition in the same chamber without breaking vacuum. CaF_2 with strong ionic bonds evaporates as a molecule and appears to be chemically inert to HTS [19]. The Au thin-film is needed to provide higher optical contrast when the single crystal becomes so thin that it is almost 100 % transparent for visible light while the intermediate CaF_2 layer is needed to protect and isolate the Bi2212 surface from the Au layer.

By conventional photolithography and Ar-ion etching, a bow-tie shaped mesa with a micro-bridge in the center is formed on the crystal (see Fig. 1(a)). The overall thickness of the Bi2212 mesa is typically about 100 nm which is controlled by the etching time and rate. In the next step, we flip the sample and glue it by using polyimide to another sapphire substrate, sandwiching the single crystal between the two substrates. Separating the substrates cleaves the single crystal into two pieces. One piece has the mesa at the bottom which is now upside down and faces the substrate. We remove all material but the mesa by iteratively cleaving the former with the aid of Scotch tape and inspecting the resulting sample in an optical

microscope. The schematic view of the resulting sample where the stand-alone “ex”-mesa is only left is shown in Fig. 1(b).

Another Au layer is then deposited and patterned immediately after that to make four gold electrodes to this tiny piece of the single crystal (micro crystal)(see Fig. 1(c)). Usually we slightly “over” etch this Au layer to make sure that no residue of gold is left on the surface between the electrodes. The micro-bridge and other areas of the micro crystal outside the electrodes therefore get slightly thinner. The micro-bridge is further thinned down by the subsequent Ar-ion etching, while electrodes and areas in between are usually protected from etching by an additional patterned CaF_2 layer (see Fig. 1(d))

Using these contacts, we could continuously measure the resistance of the bridge *in situ*, during the etching at room temperature. The superconducting properties of the sample were measured after each etching in a separate cryogenic system.

III. SAMPLE TOPOGRAPHY

Fig. 2 shows optical images of a sample illuminated from the top (a) and bottom (b). The width of the micro-bridge is 3.5 microns and the open area at the bridge for further thinning is 7 microns long. The contrast of the images is high owing to the gold thin film in the bottom of the structure.

It is quite important to assure that the Ar-ion etching is uniform. Atomic force microscopy (AFM) was used to examine the surface topography of one of the fabricated 30 nm thick micro-bridges. Fig. 3 shows an AFM image across a $5 \times 5 \mu\text{m}^2$ large area of a wider micro-bridge. The surface of the bridge is quite flat with an rms roughness of 0.28 nm and a mean surface roughness of 0.21 nm. This roughness is quite close to the freshly cleaved surface of a Bi2212 single crystal with an rms surface roughness of 0.20 nm [20]. For Bi2212 thin films with a similar thickness prepared by MBE, the mean surface roughness is between 0.5 and 0.9 nm across an area of $10 \times 10 \mu\text{m}^2$ [21]. It is clear that even after the Ar-ion etching the surface quality of the single crystals is better than that of thin films of comparable thickness grown by MBE. The surface quality of several samples of different thicknesses was examined, all with about the same result.

IV. ELECTRONIC MEASUREMENTS AND DISCUSSIONS

The electrical transport measurements of the micro-bridges were carried out in a temperature range of 16 – 290 K. Fig. 4 shows the $R - T$ curves of a micro-bridge with a $3.5 \times 3.5 \mu\text{m}^2$ large unmasked area in the middle of the bridge after each of the subsequent etchings. Despite the vanishingly small thickness, the micro-bridges are very stable and withstand more than ten cycles of cooling down from room temperature to 16 K without any noticeable change in their resistance.

The typical etching parameters used in the experiment are 230 V for the Ar-ion acceleration voltage and 0.11 mA/cm^2 ($7 \times 10^{14} \text{ s}^{-1}\text{cm}^{-2}$) for the beam current density, resulting in an etching rate α of about 1.5 nm/min or about half a unit cell in c -axis per minute.

When the total etching time is less than 40 minutes, the superconducting critical temperature T_{c0} is the same as for a bulk single crystal (~ 86 K). After some additional etching for about 8 minutes, T_{c0} starts to decrease. T_{c0} rapidly decreases to 25 K after just two more minutes of etching and finally the specimen ceases to be superconductive. At the same time, the temperature dependence of the resistance changes from a metal- to a more semiconductor-like behavior above T_c , and shows the presence of a Superconductor-Insulator (S-I) transition below T_c .

The S-I transition is an important issue in condensed matter physics [22]. For an ultrathin film, the S-I transition occurs when the sheet resistance R_{\square} is about or larger than the universal quantum value $R_q = h/4e^2 \approx 6.5 \text{ k}\Omega$ [5, 6].

The most resistive part of the bridge is the etched (and thinnest) square area $3.5 \times 3.5 \mu\text{m}^2$ in the middle of the bridge, and the resistance of the other parts in the bridge is much smaller and negligible compared with the resistance in the middle part. As a result, the resistance which we measure is close to the sheet resistance $R_{\square}(d)$ for the thinnest bridge. The quantum resistance is indicated by an arrow in Fig. 4, and we see that the boundary value for S-I transition in our samples is consistent with R_q . Similar S-I transition was also observed in other HTS ultrathin films [8, 23, 24].

Given that the etching rate is constant, we can calculate the thickness of the bridge from the etching time provided we know an initial thickness of the bridge. Although we could roughly measure the initial thickness by, say, AFM, the absolute error would be too large for a self-consistent analysis of the resistance measurements for different thicknesses.

The polyimide layer which is used to glue the micro-bridge to the substrate is not flat and sufficiently smooth to be used as the reference plane in the thickness measurements of the micro-bridge.

Nonetheless, we can use the whole set of resistance-vs-etching time data to deduce the unknown initial thickness assuming the uniform in-plane resistivity ρ_{ab} . The total resistance of the micro-bridge R consists of two parts, the in-plane resistance R_t of the middle thinner part and the resistance R_s of the two surrounding thicker parts. Strictly speaking, we should take into account some contribution from the c -axis resistivity also because the electrodes are only attached to one side of the highly anisotropic single crystal and the bias current should flow along the c -axis before getting into the bridge [25]. However, since the area of the electrodes is relatively large, we can ignore this contribution and assume it is just a small part of R_s .

Let the thinner middle part of the bridge be a slab with the width w , thickness d and length l . Its resistance $R_t = \rho_{ab}l/wd = \rho_{ab}/d$ for $l = w$ (square). The thickness is assumed to be a linear function of the etching time t : $d = d_0 - \alpha t = \alpha(t_0 - t)$, where d_0 is the initial thickness and t_0 is the total time needed to etch clear through it. The total resistance is $R(t) = R_s + \rho_{ab}/\alpha(t_0 - t)$.

This equation is used to fit the experimental $R(t)$ from Fig.4 using R_s , ρ_{ab} , and t_0 as fitting parameters. $\alpha = 1.5$ nm/min was accurately measured in a separate experiment. As is seen in Fig.5, the fit is quite good for etching times up to 48 min, while it becomes worse for times longer than that. This can be due both to the close proximity to the S-I transition and possibly to deteriorated properties of the last $(\text{CuO}_2)_2$ layer. In the latter case, the last $(\text{CuO}_2)_2$ layer had once been the surface layer before the CaF_2 layer was deposited on it, see above. Inevitable exposure to moisture in the air can result in worsening of the surface layer [26, 27].

From previous experience and present measurements, we know that there is no more than *one* surface layer which is usually affected by moisture or by the contact to a normal metal. This can easily be verified from measuring the $I - V$ curves of a stack of IJJ in a three-probe measurement at low temperatures, see for instance Fig. 2a in Ref. [26]. Only the first branch which corresponds to the surface junction has a reduced critical current. The adjacent junction already has the nominal critical current equal to the critical current of the majority of junctions in the stack.

From the best least-squares fit, ρ_{ab} , R_s , and t_0 could be determined, see Fig. 5. The in-plane resistivity ρ_{ab} at 273 K is about $8 \times 10^{-4} \Omega \cdot \text{cm}$, which is close to ρ_{ab} reported elsewhere [28, 29]. Knowledge of t_0 and α allows us to determine the precise thickness corresponding to each etching time. The initial thickness can be also calculated to be about 80 nm, which is not far from the estimations based on the etching time in the first step of the mesa fabrication, see Fig. 1a above.

Fig. 6 shows the variation of T_{c0} with the thickness expressed both in nm and the number of unit cells. When the ultrathin Bi2212 single crystal has more than 8 $(\text{CuO}_2)_2$ -layers (12 nm or 4 unit cells thick), it has the same T_c as the bulk. $T_c(d)$ starts to decrease when it is thinner than 4 unit cells, but superconductivity with finite $T_{c0} = 25$ K still persists even when there are just 1.5 unit cells left (~ 5 nm). The suggested S-I transition occurs in a slightly thinner bridge (3 nm). We have to mention here that the thickness we obtained from the curve fitting is an effective value. The physical thickness should include the thickness of a surface insulating layer formed in the ion etching process, which is no more than 3 nm [30].

Our result that the superconductivity of ultrathin Bi2212 single crystals vanishes suggests that these are intrinsically disordered. This is in agreement with several STM studies (Ref. 31, for instance) revealing short-range disorder in Bi2212 single crystals cleaved at cryogenic temperatures, as well as with other experiments on Bi2212 thin films demonstrating S-I transition [7, 8]. However, experiments with ultrathin $\text{YBa}_2\text{Cu}_3\text{O}_{7+\delta}$ (YBCO) films sandwiched between PrBCO buffer layers showed that a one-unit-cell-thick YBCO film had a non-zero $T_{\text{KT}} \approx 30$ K [32]. This can be due to better quality of RHEED-controlled YBCO epitaxial films showing less disorder but might also be due to the presence of relatively thick and electrically conducting PrBCO buffer- and cap layers.

V. CONCLUSIONS

With conventional micro-fabrication processing high-quality ultrathin Bi2212 single crystals were fabricated and studied. Superconductivity was observed for all thicknesses down to effectively 1.5 unit cells. In the thinner crystals, the superconductivity quenches while $R(T)$ changes from a metallic to a semiconductor-like behavior, suggesting a superconductor-insulator transition that takes place around $R_{\square} \sim R_q = 6.5 \text{ k}\Omega$.

Acknowledgments

We thank M. Torstensson and D. Lindberg for technical assistances and fruitful discussions. This work is financed by The Swedish Foundation for Strategic Research (SSF) through the OXIDE program.

- [1] R. Kleiner, F. Steinmeyer, G. Kunkel, P. Muller, **68**, 2394 (1992).
- [2] M. P. A. Fisher, Phys. Rev. Lett. **65**, 923 (1990).
- [3] D. B. Haviland, Y. Liu, and A. M. Goldman, Phys. Rev. Lett. **62**, 2180 (1989).
- [4] M-C. Cha, M. P. A. Fisher, S. M. Girvin, M. Wallin, and A. P. Young, Phys. Rev. B **44**, 6883 (1991)
- [5] H. M. Jaeger, D. B. Haviland, A. M. Goldman, B. G. Orr, Phys. Rev. B **34**, 4920 (1986).
- [6] R. A. Ferrell, B. Mirhashem, B **37** 648, (1986).
- [7] H. Ota, S. Migita, Y. Kasai, H. Matsuhata, S. Sakai, Physica C **311**, 42 (1999).
- [8] Y. Qi, K. Sakai, H. Murakami, J. Low. Temp. Phys. **117**, 669 (1999).
- [9] P. Bove, D.J. Rogers, F. Hosseini Teherani, J. Crystal Growth **220**, 68 (2000).
- [10] I. Bozovic, IEEE Trans. Appl. Supercond. **11**, 2686 (2001).
- [11] M. Ohring, The Materials Science of Thin Films, (Academic Press, San Diego 2002).
- [12] V. Hardy, A. Wahl, A. Ruyter, A. Marignan, C. Nartin, L. Coudrier, J. Provost, C. Simon, Physica C **232**, 347 (1994).
- [13] M. Pissas, B. Billon, M. Charalambous, J. Chaussy, S. LeFloch, P. Borde, J. J. Capponi, Supercond. Sci. Technol. **10**, 598. (1997)
- [14] C. T. Lin, M. Freiberg and E. Schön herr: Physica C **337**, 270 (2000).
- [15] X. Yao, A. Hu, Supercond. Sci. Technol. **17**, L47 (2004).
- [16] H. B. Wang, J. Chen, L. X. You, P. H. Wu, T. Yamashita, IEICE Trans. Electron. **E85-c**, 691 (2002).
- [17] L. X. You, P. H. Wu, W. W. Xu, Z. M. Ji, L. Kang, Jpn. J. Appl. Phys. Part 1 **43(7A)**, 4163 (2004).
- [18] L. X. You, P. H. Wu, J. Chen, W. W. Xu, K. Kajiki, S. Watauchi, I. Tanaka, Supercond. Sci. Technol. **17**, 1160 (2004).

- [19] D. M. Ginsberg, *Physical Properties of High Temperature Superconductors II*, (World Scientific, Singapore, 1990).
- [20] L. X. You, A. Yurgens, D. Winkler, *Phys. Rev. B* **71**, 224501 (2005).
- [21] P. Bove, D. J. Rogers, F. H. Teherani, *J. Crystal Growth* **220**, 68 (2000).
- [22] M. Imada, A. Fujimori, Y. Tokura, *Rev. Mod. Phys.* **70**, 1039 (1998).
- [23] U. Kabasawa, Y. Tarutani, T. Fukazawa, N. Sugii, H. Hasegawa, K. Takagi, *J. Appl. Phys.* **10**, 7849 (1996).
- [24] M. Salluzzo, A. Cassinese, G. M. De Luca, A. Gambardella, A. Prigiobbo, R. Vaglio, *Phys. Rev. B* **70**, 214528 (2004).
- [25] R. Busch, G. Ries, H. Werthner, G. Kreiselmeyer, and G. Saemann-Ischenko, *Phys. Rev. Lett* **69**, 522 (1992).
- [26] N. Kim, Y.-J. Doh, H.-S. Chang, and H.-J. Lee, *Phys. Rev. B* **59**, 14639 (1999).
- [27] X. B. Zhu, S. P. Zhao, G. H. Chen, H. J. Tao, C. T. Lin, S. S. Xie, and Q. S. Yang, *Physica C* **403**, 52 (2004).
- [28] J. R. Cooper, L. Forro, B. Keszei, *Nature* **343**, 444 (1990).
- [29] T. Watanabe, T. Fujii, A. Matsuda, *Phys. Rev. Lett.* **79**, 2113 (1997).
- [30] L. X. You, P. H. Wu, Z. M. Ji, S. X. Fan, W. W. Xu, L. Kang, C. T. Lin and B. Liang, *Supercond. Sci. Technol.* **16**, 1 (2003).
- [31] K. M. Lang, V. Madhavan, J. E. Hoffman, E. W. Hudson, H. Eisaki, S. Uchida and J. C. Davis, *Nature* **415**, 412 (2002).
- [32] Y. Matsuda, S. Komiyama, T. Onogi, T. Terashima, K. Shimura, and Y. Bando, *Phys. Rev. B* **48**, 10498 (1993).

Figure Captions

Figure 1. (Color online) Schematic view of the patterning steps for the micro-crystal and a bridge in the center.

Figure 2. (Color online) (a), (b) Optical images of a sample illuminated from the top and bottom respectively. Indicated in the images are I) the gold contact, II) the Bi2212 micro-bridge, III) the CaF₂ layer and IV) the substrate. All the gold contacts and the micro-bridge are protected by CaF₂, except for the rectangle ($7 \times 3.5 \mu\text{m}^2$) in the middle of the bridge.

Figure 3. (Color online) The AFM image over an area of $5 \times 5 \mu\text{m}^2$ on a Bi2212 micro-bridge. The thickness of the bridge is about 30 nm. The inset shows the surface profile along an arbitrarily chosen direction.

Figure 4. (Color online) RT curves of a BSCCO micro-bridge with the open area $3.5 \times 3.5 \mu\text{m}^2$ after subsequent etching times. The initial thickness of the bridge is less than 90 nm.

Figure 5. Resistance ($T = 273 \text{ K}$) of the micro-bridge vs. the etching time (dots) fitted by $R(t) = R_s + \rho_{ab}/\alpha(t_0 - t)$ (solid line). Best-fit parameters are shown in the inset. $\alpha = 1.5 \text{ nm/min}$ was measured in separate experiments.

Figure 6. Variation of T_{c0} with the thickness of the bridge (number of unit cells) in c -axis direction.

Figures

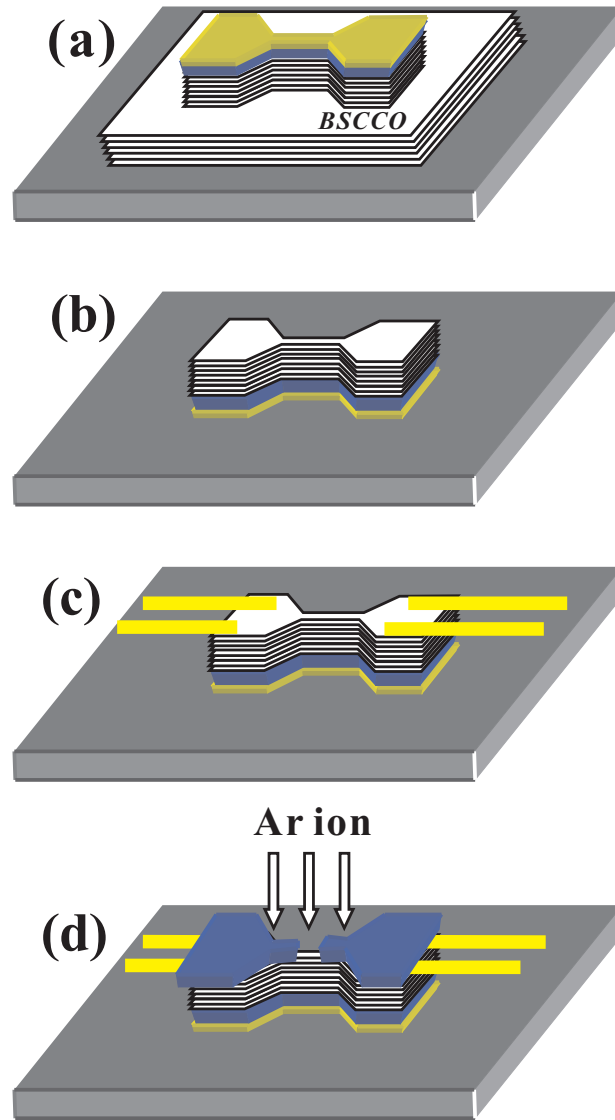


FIG. 1: (Color online) Schematic view of the patterning steps for the micro-crystal and a bridge in the center.

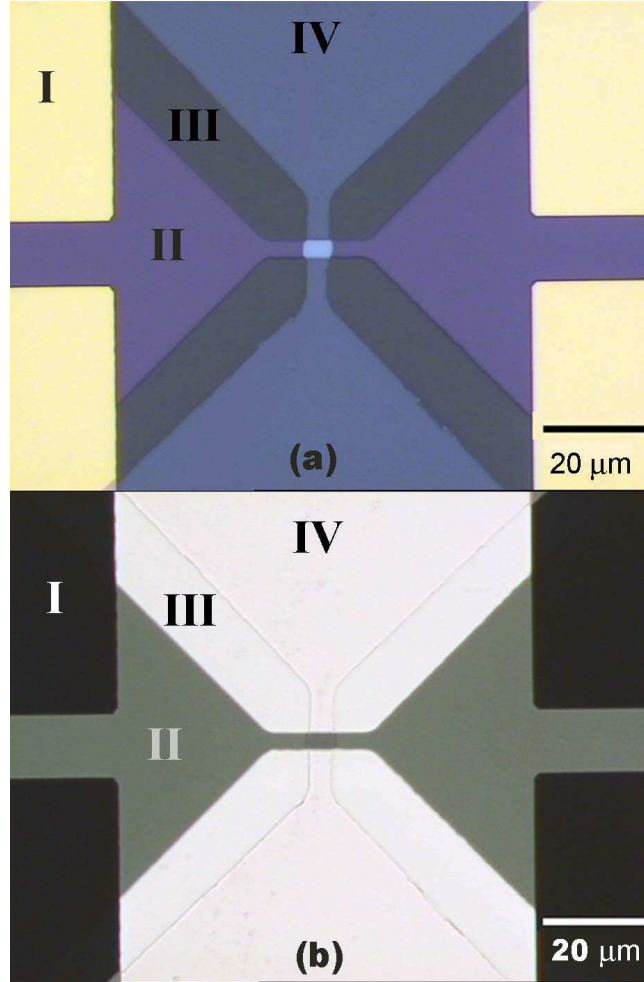


FIG. 2: (Color online) (a), (b) Optical images of a sample illuminated from the top and bottom respectively. Indicated in the images are I) the gold contact, II) the Bi2212 micro-bridge, III) the CaF_2 layer and IV) the substrate. All the gold contacts and the micro-bridge are protected by CaF_2 , except for the rectangle ($7 \times 3.5 \mu\text{m}^2$) in the middle of the bridge.

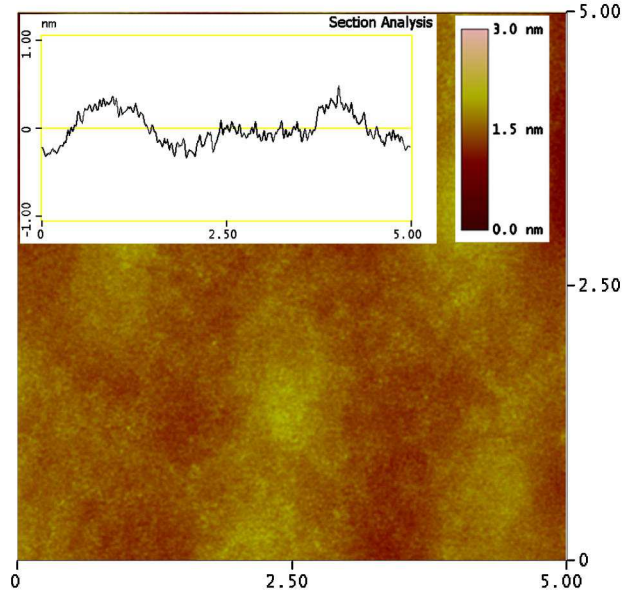


FIG. 3: (Color online) The AFM image over an area of $5 \times 5 \mu\text{m}^2$ on a Bi2212 micro-bridge. The thickness of the bridge is about 30 nm. The inset shows the surface profile along an arbitrarily chosen direction.

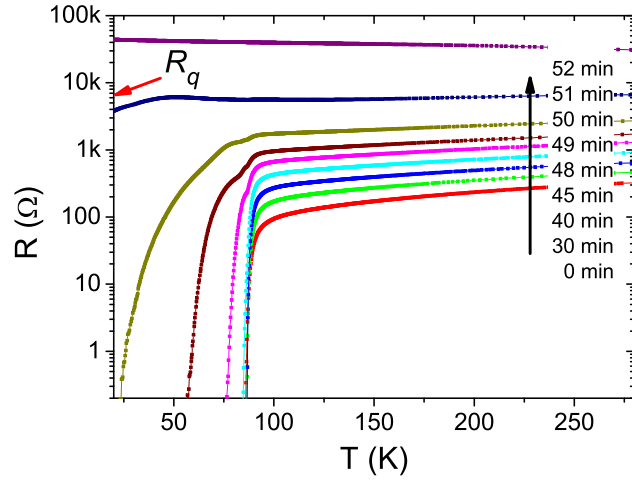


FIG. 4: (Color online) RT curves of a BSCCO micro-bridge with the open area $3.5 \times 3.5 \mu\text{m}^2$ after subsequent etching times. The initial thickness of the bridge is less than 90 nm.

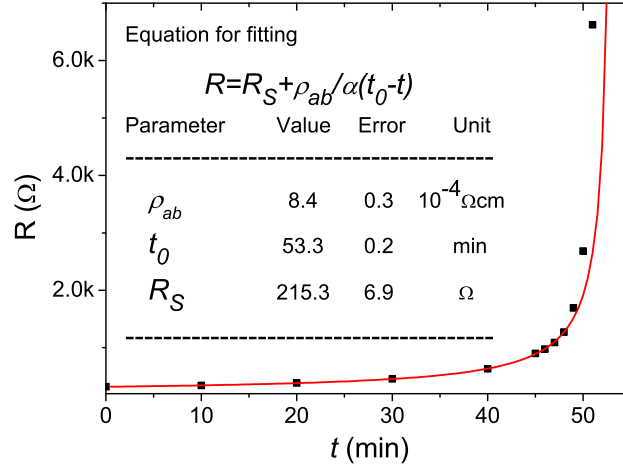


FIG. 5: Resistance ($T = 273 \text{ K}$) of the micro-bridge vs. the etching time (dots) fitted by $R(t) = R_s + \rho_{ab}/\alpha(t_0 - t)$ (solid line). Best-fit parameters are shown in the inset. $\alpha = 1.5 \text{ nm/min}$ was measured in separate experiments.

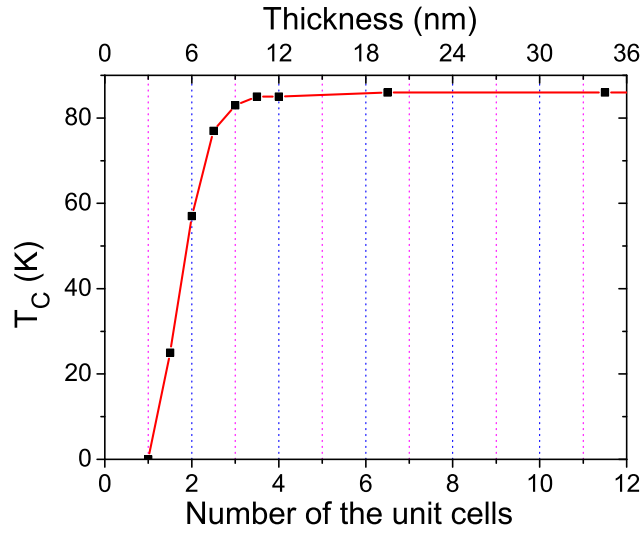


FIG. 6: Variation of T_{c0} with the thickness of the bridge (number of unit cells) in c -axis direction.